Labyrinth pattern in a decagonal quasicrystal

Author(s):
He, Zhanbing; Wang, Yanguo; Zhang, Tiantian; Huang, Shuzhao; Steurer, Walter

Publication date:
2023-09-20

Permanent link:
https://doi.org/10.3929/ethz-b-000633081

Originally published in:
Cell Reports Physical Science 4(9), https://doi.org/10.1016/j.xcrp.2023.101578

Cell Reports
Physical Science

CellPress
OPEN ACCESS

Article

Labyrinth pattern in a decagonal quasicrystal

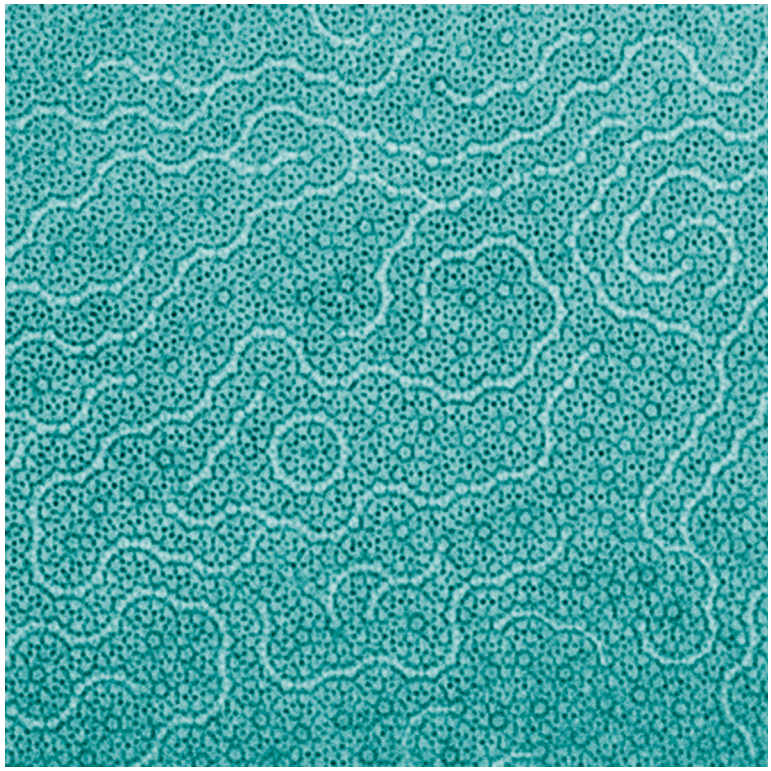

He et al. report labyrinth patterns of quasicrystal in $Al_{68}Cr_{26}Si_6$, as shown by TEM. The arrangement of the domain walls resembles that of ferroelectric or magnetic domain structures, although these are of different origin and on different scales. The labyrinth patterns of quasicrystals have the potential for exploring materials with unusual properties.

Zhanbing He, Yanguo Wang, Tiantian Zhang, Shuzhao Huang, Walter Steurer

hezhanbing@ustb.edu.cn

Highlights

The labyrinth patterns of quasicrystals are discovered

The walls of labyrinth patterns of quasicrystals consist of hexagons

The curve walls of labyrinth can be switched to straight by heating

He et al., Cell Reports Physical Science 4, 101578
September 20, 2023
https://doi.org/10.1016/j.xcrp.2023.101578

Cell Reports
Physical Science

CellPress
OPEN ACCESS

Article

Labyrinth pattern in a decagonal quasicrystal

Zhanbing He,[1,4,*] Yanguo Wang,[2] Tiantian Zhang,[1] Shuzhao Huang,[1] and Walter Steurer[3]

SUMMARY

The unique properties of quasicrystals are closely related with their complex crystal structures and microstructures. Here, we report the labyrinth structures of decagonal quasicrystal in $Al_{68}Cr_{26}Si_6$, which is scarcely found in quasicrystals. An electron microscopic study of as-cast $Al_{68}Cr_{26}Si_6$ shows a structure of quasiperiodic nanodomains with overall decagonal diffraction symmetry. The quasiperiodic nanodomains are separated by a labyrinthine pattern of edge-connected structural building blocks shaped like squashed (fat) hexagons. The arrangement of the domain walls resembles that of ferroelectric or magnetic domain structures, although these are of different origin and on different scales. By annealing $Al_{68}Cr_{26}Si_6$ at 1,223 K, the domain wall density is strongly increased and appears to be arranged periodically in a specific way.

INTRODUCTION

Labyrinths have been widely built for fun in our macro world, but labyrinthine patterns are also quite common in the microstructures of magnetic materials,[1] ferroelectrics,[2] and even in ice crystals during irradiation,[3] for instance, but they have not been observed in quasicrystals so far. For a theoretical study on labyrinth formation and transformation, see, e.g., Echeverría-Alar's work.[4] Generally, domain structures on the micro- or nanoscale can have influence on the physical and mechanical properties of materials. They may have potential for exploring novel materials with unusual properties, for developing nanotechnologies such as nanolithography and nanoelectricity,[5] for instance.

The discovery of quasicrystals by Shechtman et al.[6] has garnered great interest in their strange crystal structures, defects, and unusual physical properties they may have. For a review, see, e.g., Steurer's work.[7] We will focus on decagonal quasicrystals (DQCs), because this is relevant to the samples of $Al_{68}Cr_{26}Si_6$ we studied. Generally, the structures of quasicrystals can be discussed in terms of structural building blocks or geometrical clusters, respectively.[8] The shapes of the basic structural building blocks of DQCs can be described by decagons (D), pentagons (P), hexagons (H), stars (S), rhombi (R), bow-ties (T), or boats (B), which have been widely found in Al-based DQCs,[7–13] for instance. Consequently, by specific combinations of these basic structural subunits, the structures of DQCS can be described as well as those of their approximants and defect structures.[14,15] Although different types of structural defects[16–23] have been found in quasicrystals, the counterparts to the labyrinthine domain patterns in crystals have not been observed in quasicrystals before our study (see, e.g., Honal et al.[24] and references therein).

We want to have a closer look at decagonal Al-Cr-Si, which was described to exist as metastable phase next to a metastable icosahedral quasicrystal.[25,26] In the ternary Al-Cr-Si phase diagram,[27] taken at 1,073 K, metastable phases are not included.

[1]State Key Laboratory for Advanced Metals and Materials, University of Science & Technology Beijing, Beijing 100083, China

[2]Institute of Physics, Chinese Academic of Science, Beijing, China

[3]Department of Materials, ETH Zurich, 8093 Zurich, Switzerland

[4]Lead contact

*Correspondence: hezhanbing@ustb.edu.cn

https://doi.org/10.1016/j.xcrp.2023.101578

However, the composition of our sample, $Al_{68}Cr_{26}Si_6$, is close to that of hexagonal τ_2-$Al_{68}Cr_{24.5}Si_{7.5}$ at 1,073 K.

By means of transmission electron microscopy, we discover the labyrinth domains of decagonal quasicrystal in an $Al_{68}Cr_{26}Si_6$ alloy. Meanwhile, the quasiperiodic domain structure is found to be coherent even over the labyrinthine domain walls. This means that at least a quasiperiodic coincidence sublattice exists, which is reflected in the decagonal diffraction symmetry. Since quasiperiodic tilings are known in many examples of the medieval Islamic architecture,[28] the labyrinthine pattern of quasicrystals may also find potential applications not only in the design of new materials and nanotechnologies but also in architecture and for artificial labyrinths in the macro world.

RESULTS AND DISCUSSION

As-cast sample

Figure 1A shows a high-resolution transmission electron microscopy (HRTEM) image of the labyrinthine domain-wall structure of decagonal $Al_{68}Cr_{26}Si_6$ taken at overfocus and with the contrast inversed for better displaying the domain walls (highlighted in white). Note that all the original images without tiling in the paper are shown in the supplemental information (see Figures S1–S5). There are many nanoscale domain variants separated by the domain boundaries with different curvatures, leading to the formation of a complex domain structure with a labyrinthine pattern. The domain labyrinth has a close relation with the distribution of the nanoscale domain variants, because these irregularly arranged domain variants act as its components, resulting in the observable labyrinthine pattern. Generally, coarsening of quasicrystalline grains in decagonal $Al_{68}Cr_{26}Si_6$ alloys has a close relation to the size of domain variants, and consequently, the number of domain variants directly depends on the number of these remained grains. It can be concluded from the diffraction characteristic of a single crystal of this DQC in Figure 1C that the domain variants in Figure 1A have the same crystallographic orientations. However, the mismatch between the neighboring variants at their interfaces makes the domain boundaries to be out of phase. The presence of the out of phase boundaries confines the coarsening of the domain variants via merging of the neighboring variants. It results in a structural discontinuation between the neighboring variants, leading to the formation of many nanoscale domain variants and the domain labyrinth. Some domain walls are connected at specific nodes and then separating again. In addition, some decagonal structure motifs, with a circumscribed circle diameter of 3.45 nm, resemble the famous Longleat Safari Park Labyrinth.

The HRTEM image in Figure 1B, taken at underfocus, shows the tiling structure of a few nanodomains and domain walls from the area inside the crop marks in Figure 1A. The labyrinth walls in Figure 1B correspond to those in Figure 1A. They are marked by white segments passing through the waists of the fat (squashed) hexagons (H_F) with edge lengths of 0.65 nm (some hexagons are marked in green as an example). The basic structural blocks in between the walls are mainly quasiperiodically covered by S and H tiles with the same edge length of 0.65 nm. All tiles appear only in the five characteristic orientations, differing by $n.360°/5 = n.72°$. All labyrinth domain walls start from (or end at) the center of S tiles. The sky-blue D tile (with a circumscribed circle diameter of 2.12 nm) in the left part of Figure 1B has the same edge lengths as the S and thin H tiles. However, the diameter of the D tile may be scaled up by a factor τ times to 3.45 nm, when the waists of the H_F tiles surrounding the 2.12-nm D tile are connected (Figure 1A). Figure 1C depicts the fast Fourier transform of Figure 1B, where the diffraction spots are relatively sharp but accompanied by

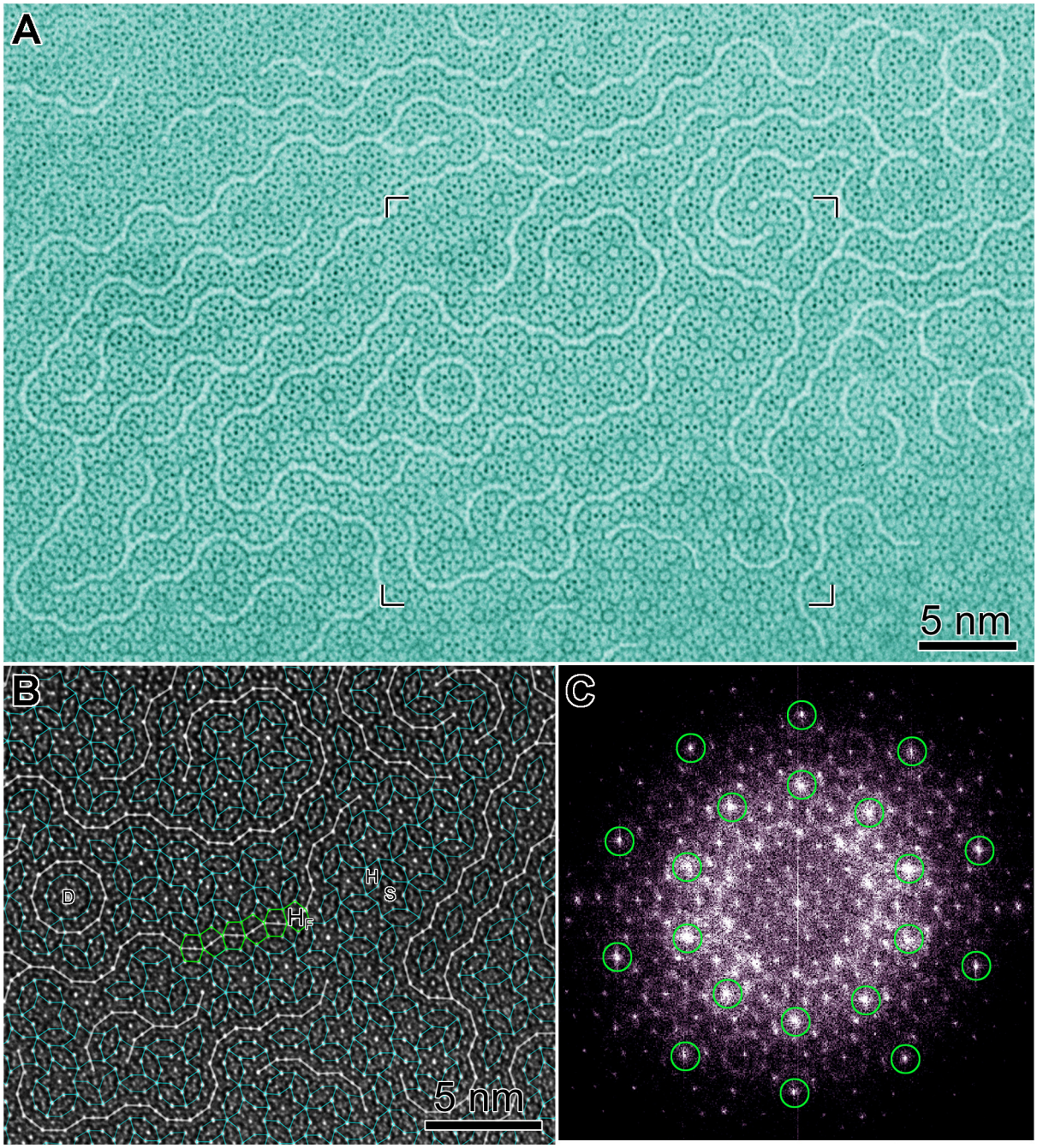

Figure 1. Labyrinth pattern in decagonal as-cast $Al_{68}Cr_{26}Si_6$ revealed by high-resolution transmission electron microscopy (HRTEM) imaging

(A) HRTEM image, taken under defocus, where the labyrinth walls are highlighted in white.

(B) Corresponding HRTEM image from the marked center area in (A), where the labyrinth walls are marked by white line segments. The basic structural units, hexagons (H) and stars (S), in between the walls are outlined in sky blue. Structure motifs (H_F) around some segments of the labyrinth lines are marked in green.

(C) Fast Fourier transform of the HRTEM image in (B). The strong diffraction spots clearly display 10-fold symmetry indicating an on-average quasiperiodic structure.

diffuse scattering, indicating some amount of disorder. The diffraction spots are distributed as is characteristic for DQCs, with the strong peaks being arranged with typical 10-fold symmetry.

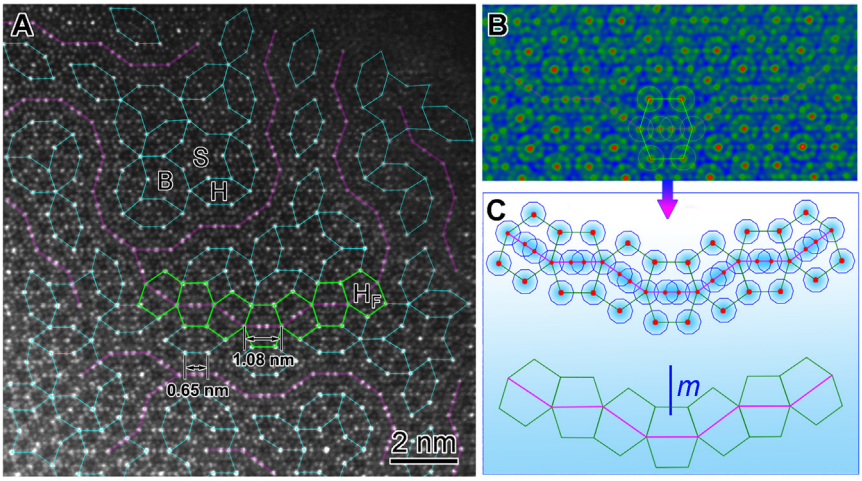

Figure 2. High-angle annual dark-field scanning transmission electron microscopy (HAADF-STEM) image visualizing the labyrinth pattern in our DQCs

(A) Tiling pattern of the labyrinth as revealed from the HAADF-STEM image. The labyrinth walls consist of just H_F tiles (outlined in green). The positions of the walls are indicated by pink lines, which pass through the middle lines of the H_F tiles.

(B) Enlarged and Fourier filtered HAADF-STEM image from the area marked by the green H_F tiles in (A).

(C) Schematic of the wall in (B) The overlapped smallest decagons produce a wall of decagons without gaps, as indicated by the thick pink lines passing through the centers of the smallest decagons. Interestingly, a local mirror symmetry (m) exists in the wall, as seen in the lower row of (C).

To further reveal the structural details of the labyrinth, we carried out high-angle annual dark-field scanning transmission electron microscopy (HAADF-STEM) studies, as shown in Figure 2A. The smallest structural blocks correspond to the wheel-like contrasts, with one white spot surrounded by ten relatively weak spots. Linking the centers of these clusters yields the basic structural units S, B, H, H_F, etc., with an edge length of 0.65 nm—the same as those in Figure 1. As we know from other studies, these wheels are projections of columns of vertex-connected icosahedral clusters. For instance, in $Al_{13}Cr_4Si_4$ and binary Al-Cr compounds, the Cr atoms are icosahedrally coordinated by Al, mainly.[29,30] The projected icosahedra in our structure then appear as a small, centered, ten-member ring at the corners of the structural building blocks. According to the imaging properties of HAADF-STEM (atomic contrast proportional to Z^2, with Z the atomic number), we can assign the bright central contrast to Cr atoms and the weak contrasts around them to Al or Si atoms.

We only mark a few parts of the labyrinth pattern with green H_F tiles for clarity, but most labyrinth walls are indicated by pink lines through the middle of H_F tiles. For clearly displaying the structures of the walls, a Fourier filtered image of a part of one wall in Figure 2A is enlarged and shown in Figure 2B. Clearly, the two smallest clusters inside the H_F tiles overlap with a rugby-ball-like shape to generate a Gummelt's B-type covering,[31,32] as schematically shown in Figure 2C. The overlapping ring contrasts arise from columns of face-connected Cr-centered icosahedral (Al, Si) clusters. Interestingly, we see a local mirror symmetry in the wall although the wall is curved (as indicated by an *m* in Figure 2C), which implies that the elongation of walls also follows certain symmetry operations, occasionally.

Annealed sample

In order to study the structural stability of the labyrinth pattern, the sample was annealed at 1,223 K for 120 h, and one typical pattern of the labyrinth after being

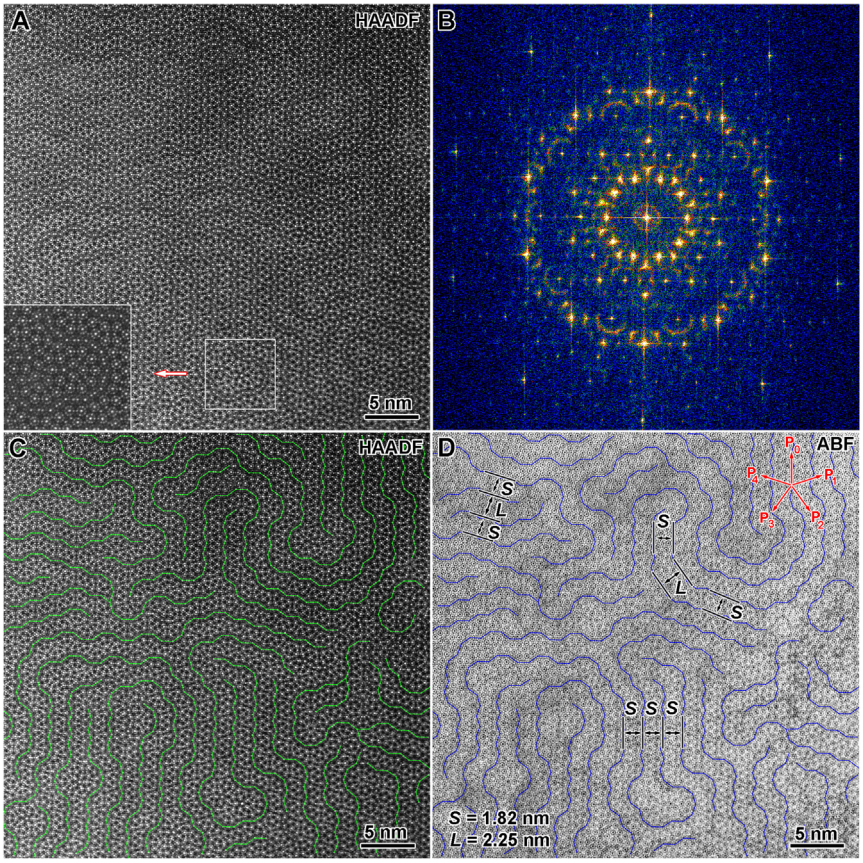

Figure 3. Typical labyrinth pattern after annealing

(A) Low-magnification HAADF-STEM image (Cr has a much brighter contrast than Al, Si) with an enlarged image at bottom left.

(B) Fast Fourier transform of the image in (A), where the strong diffraction spots still display 10-fold symmetry.

(C) The walls of the labyrinth in the HAADF-STEM image in (A) are highlighted by green lines for better visualization.

(D) The corresponding annular bright-field (ABF) image using STEM (Cr, Al, Si have comparable contrasts).

annealed is shown in Figure 3. It shows a low-magnification HAADF-STEM image (contrast proportional to Z^2). The labyrinth walls observable in Figure 3A are marked in green in the HAADF-STEM image (Figure 3C) and in blue on the annular bright-field (ABF)-STEM image (contrast proportional to $Z^{1/3}$) (Figure 3D). Compared to the domain walls in Figure 1, much more parallel walls have been generated, where most of them align along the direction of P_0 and a few along P_4, with the P_0 and P_4 differing by 72° (marked in Figure 3D). The labyrinth walls appear to be continuous and extend densely all over the two-dimensional plane. The distances between parallel walls are either $S = 1.82$ nm or $L = \tau S = 2.25$ nm, whereby S distances are dominating. During annealing, the labyrinthine structure was thermally excited by the activation energy K_BT (~0.105 eV at 1,223K), where $K_B = 1.38 \times 10^{-23}$J/K and T are the Boltzmann constant and absolute temperature of the annealed labyrinthine pattern respectively. If the activation energy is close to height of the potential barrier between the different domain patterns, the original labyrinthine structure can change from one pattern to another configuration after a long time at the annealing temperature. As a result, a pattern

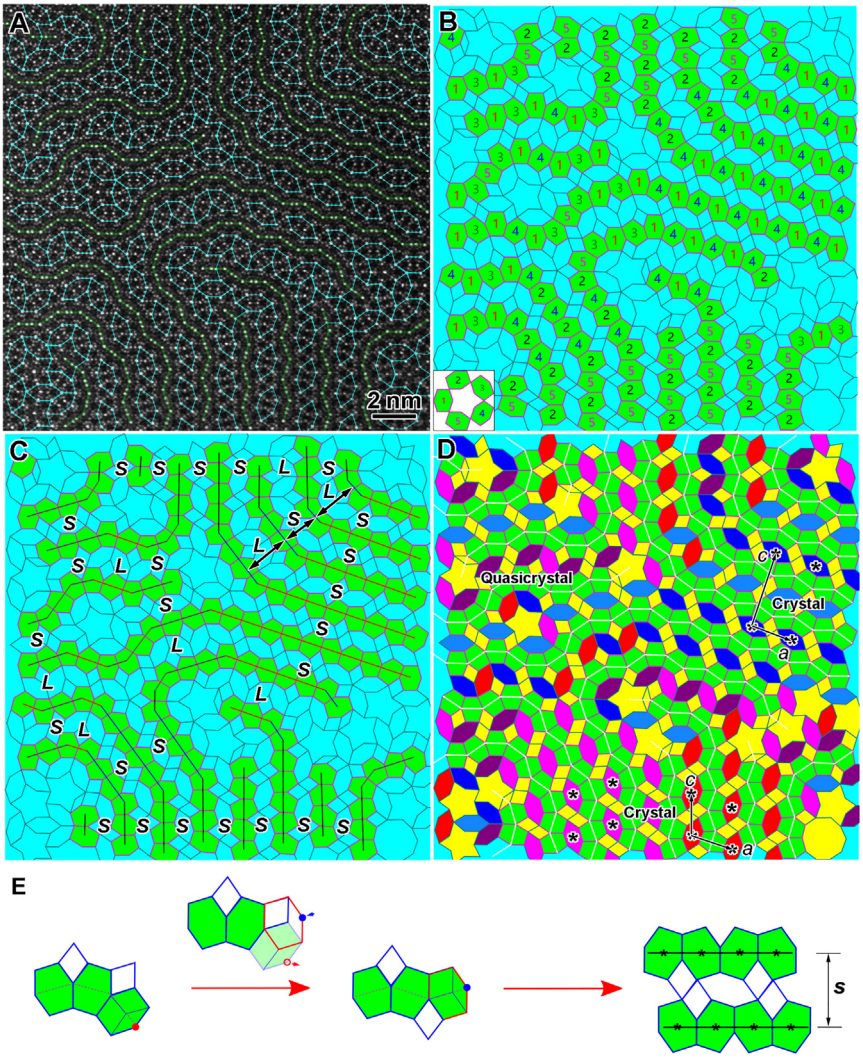

Figure 4. Labyrinth structure after annealing

(A) Enlarged HAADF-STEM image adopted from the center in Figure 3A.

(B) The five orientations of H_F tiles, marked by "1, 2, 3, 4, 5."

(C) Tiling illustrating the local periodicities of the domain walls (shaded green).

(D) Tiling illustrating the coherent intergrowth of periodic and quasiperiodic areas.

(E) The structural evolution of curve wall to straight wall through atomic jumps. The nearby straight walls can produce a distance "*S*," as largely observed in Figure 4A.

reconstruction of the domain labyrinth happened, and the different configuration of the labyrinth pattern with respect to Figure 1A appeared after annealing. After such a pattern reconstruction, the resulted labyrinthine domain should be stable at 1,223K with respect to the original labyrinth pattern.

An enlarged image containing both parallel and curved walls is shown in Figure 4 for a detailed analysis. Figure 4A is an HAADF-STEM image, and the corresponding structural tiling is depicted in Figures 4B–4D. For clarity, there the domain walls are filled in green and the matrix in sky-blue in Figures 4B and 4C for clarity. There are five orientations of H_F tiles (marked as 1, 2, 3, 4, 5 in Figure 4B). Interestingly, the combinations of two of five oriented H_F tiles, for example the combinations of "1" and "4" H_F tiles appearing at top-right as well as that of "2" and "5" found in the

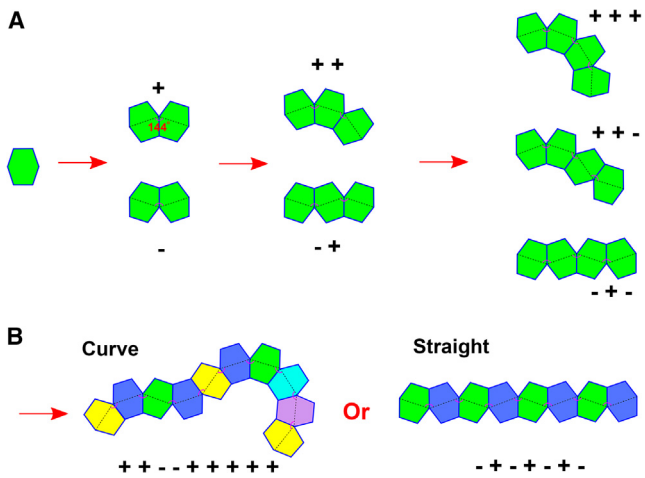

Figure 5. Growth rules for the labyrinth walls

(A) There are only two combinations for three edge-sharing H_F tiles: the 144° turning angle located at the same or at the opposite side of the middle lines of H_F tiles (marked by dashed lines), represented by "+ +" and "– +", respectively. The middle lines of H_F tiles in the wall must be continuous.

(B) The continuous "+" or "–" will generate a curved wall, but alternative "+" and "–" will lead to a straight wall. In other words, there are more than two orientations of H_F tiles in the curve wall but only two orientations of H_F tiles in the straight wall. H_F tiles orientations are indicated by different colors.

bottom, generate straight walls, whereas more than two oriented H_F tiles in one wall bring locally curved walls, as seen in Figure 4C. The period *S* between the walls is found at right and the bottom. Consequently, crystalline areas are found where the walls are parallel; for example, one orthorhombic unit cell with a = 1.95 nm, c = 3.66 nm at right and one monoclinic unit cell with $a = c$ = 1.95 nm, β = 108° are outlined in the bottom right of Figure 4D, respectively. At left, a disordered quasiperiodic tiling structure can be seen. Remarkably, there are just coherent domain walls between the quasicrystal and crystal areas, which are reflected by the coherent connections of structural blocks. Upon annealing, phason flipping could happen,[33,34] resulting in the transformation from the curved walls of H_F tiles to straight walls, which can further generate the spaces *S* or *L* locally, as shown in Figure 4E. From the energy point of view, the transformation from curved to straight walls will enhance the stability of the system because the interface energy of straight walls is generally lower than that of curved walls via decreasing the interfacial areas.

The orientation relationships of the H_F in the labyrinth walls are discussed geometrically in Figure 5. Basically, two edge-connected H_F tiles are tilted by 36° relative to one another leading to a 144° kink for the equatorial lines within them (dashed lines). Note that we use "+" and "–" to distinguish the orientations of two neighboring H_F tiles. Consequently, the combination of three edge-connected H_F tiles can generate two different configurations: one with two 144° angles located at the same side of middle lines of H_F tiles and another with two 144° angles located at the opposite side and represented by "+ +", and "– +", respectively (Figure 5A). Other combinations of H_F tiles are shown in Figure 5B.

Decagonal $Al_{68}Cr_{26}Si_6$ is the first known example where such a labyrinth pattern of nanodomain walls can be observed. The nanodomains, consisting of edge-sharing

H_F tiles, on either side of the walls coherently preserve the overall decagonal symmetry, on average. The labyrinth pattern appears drastically changed after annealing the as-cast sample at 1,223 K for 120 h, where the domain walls form two different periodicities (*S* and *L*) and, therefore, extended crystalline areas besides still existing quasiperiodic nanodomains. Hopefully, the labyrinth pattern of this quasicrystal may shed some light on the exploration of new materials, the application in nanotechnology, as well as the creation of artificial labyrinths.

EXPERIMENTAL PROCEDURES

Resource availability

Lead contact

Further information and requests for resources and reagents should be directed to and will be fulfilled by the lead contact, He Zhanbing (hezhanbing@ustb.edu.cn).

Materials availability

This study did not generate new unique materials.

Data and code availability

All data analyzed during this study are present in the article or the supplemental information. This study did not generate datasets.

Material preparation

Ternary Al-Cr-Si alloys with the nominal compositions of $Al_{68}Cr_{26}Si_6$ were prepared by repeated melting of high-purity Al, Cr, and Si in an arc furnace. Some fragments of the as-cast samples were sealed in evacuated tubes for heat treatment at 1,223 K for 120 h.

Structure analysis

The microstructures of $Al_{68}Cr_{26}Si_6$ quasicrystal alloys before and after annealing are analyzed via HRTEM, HAADF-STEM, and ABF-STEM. Powder samples for HRTEM, HAADF-STEM, as well as ABF-STEM observation are adopted by grinding small pieces of bulk samples in ethanol and then dropping onto the TEM grid covered with holey carbon film. The HRTEM images and electron diffraction patterns are analyzed via the FEI Tecnai F30 transmission electron microscopes. The JEM-ARM200F microscope (operated at 200 kV, point-to-point resolution of 0.78 Å) equipped with cold field emission gun, Cs-probe corrector, and Cs-image corrector is used to analyze the HAADF-STEM images at an atomic resolution. We adopt different modes just to clearly reveal the structural characterizations of the labyrinth patterns in quasicrystals from different ways. For images taken at overfocus condition, it can clearly and intuitively demonstrate the domain walls of the labyrinth patterns; for those taken at underfocus condition, it can show clearly the typical structural blocks of quasicrystals by recognizing the bright spots in the HRTEM images, as widely adopted in the structural analysis from the HRTEM images of quasicrystals. Furthermore, the structural details and atomic types can be directly recognized from the atomic-resolution HAADF-STEM images.

SUPPLEMENTAL INFORMATION

Supplemental information can be found online at https://doi.org/10.1016/j.xcrp.2023.101578.

ACKNOWLEDGMENTS

This work is supported by the National Natural Science Foundation of China (52171151 and 51871015). This paper is also written to commemorate the 100th

anniversary of Prof. Kehsin Kuo, who was Z.B.H.'s Ph.D. supervisor and guided Z.B.H.'s study of quasicrystals from 2000 to 2005.

AUTHOR CONTRIBUTIONS

Z.B.H. conceived the idea and designed the experiments. Z.B.H., T.T.Z., and S.Z.H. participated in experimental testing. Z.B.H., W.S., and Y.G.W. wrote the manuscript. Z.B.H., Y.G.W., T.T.Z., S.Z.H., and W.S. analyzed the data, discussed the results, and drew conclusions. All authors reviewed the manuscript.

DECLARATION OF INTERESTS

Authors declare that they have no competing interests.

Received: May 8, 2023
Revised: July 27, 2023
Accepted: August 21, 2023
Published: September 12, 2023

REFERENCES

1. Heritage, K., Bryant, B., Fenner, L.A., Wills, A.S., Aeppli, G., and Soh, Y.A. (2020). Images of a first-order spin-reorientation phase transition in a metallic kagome ferromagnet. Adv. Funct. Mater. *30*, 1909163. https://doi.org/10.1002/adfm.201909163.

2. Nahas, Y., Prokhorenko, S., Fischer, J., Xu, B., Carrétéro, C., Prosandeev, S., Bibes, M., Fusil, S., Dkhil, B., Garcia, V., and Bellaiche, L. (2020). Inverse transition of labyrinthine domain patterns in ferroelectric thin films. Nature *577*, 47–51. https://doi.org/10.1038/s41586-019-1845-4.

3. Guy Preis, S., Chayet, H., Katz, A., Yashunsky, V., Kaner, A., Ullman, S., and Braslavsky, I. (2019). Labyrinth ice pattern formation induced by near-infrared irradiation. Sci. Adv. *5*, eaav1598. https://doi.org/10.1126/sciadv.aav1598.

4. Echeverría-Alar, S., and Clerc, M.G. (2020). Labyrinthine patterns transitions. Phys. Rev. Res. *2*, 042036. https://doi.org/10.1103/PhysRevResearch.2.042036.

5. Malescio, G., and Pellicane, G. (2003). Stripe phases from isotropic repulsive interactions. Nat. Mater. *2*, 97–100. https://doi.org/10.1038/nmat820.

6. Shechtman, D., Blech, I., Gratias, D., and Cahn, J.W. (1984). Metallic phase with long-range orientational order and no translational symmetry. Phys. Rev. Lett. *53*, 1951–1953. https://doi.org/10.1103/PhysRevLett.53.1951.

7. Steurer, W. (2018). Quasicrystals: What do we know? What do we want to know? What can we know? Acta Crystallogr. A *74*, 1–11. https://doi.org/10.1107/S2053273317016540.

8. Steurer, W., and Deloudi, S. (2012). Cluster packing from a higher dimensional perspective. Struct. Chem. *23*, 1115–1120. https://doi.org/10.1007/s11224-011-9864-2.

9. Steurer, W. (2004). Twenty years of structure research on quasicrystals. Part I. Pentagonal, octagonal, decagonal and dodecagonal quasicrystals. Z. Kristallogr. *219*, 391–446. https://doi.org/10.1524/zkri.219.7.391.35643.

10. Abe, E., Yan, Y., and Pennycook, S.J. (2004). Quasicrystals as cluster aggregates. Nat. Mater. *3*, 759–767. https://doi.org/10.1038/nmat1244.

11. Ma, H., He, Z., Li, H., Zhang, T., Zhang, S., Dong, C., and Steurer, W. (2020). Novel kind of decagonal ordering in $Al_{74}Cr_{15}Fe_{11}$. Nat. Commun. *11*, 6209. https://doi.org/10.1038/s41467-020-20077-4.

12. He, Z., Ma, H., Li, H., Li, X., and Ma, X. (2016). New type of Al-based decagonal quasicrystal in $Al_{60}Cr_{20}Fe_{10}Si_{10}$ alloy. Sci. Rep. *6*, 22337. https://doi.org/10.1038/srep22337.

13. Ma, H., He, Z., Hou, L., and Steurer, W. (2018). Exceptionally large areas of local tenfold symmetry in decagonal $Al_{59}Cr_{21}Fe_{10}Si_{10}$. J. Alloys Compd. *765*, 753–756. https://doi.org/10.1016/j.jallcom.2018.05.084.

14. Ma, X.L. (2002). Microdomains of decagonal approximants in $Al_{67}Cr_{15}Cu_{18}$ alloy. Phys. Status Solidi B *231*, 601–606. https://doi.org/10.1002/1521-3951(200206)231:2<601::AID-PSSB601>3.0.CO;2-6.

15. Li, H., Wang, Y., Li, G., You, L., Wang, W., Yu, R., and He, Z. (2019). 180° domain related to structurally complex crystals in $Al_{60}Cr_{20}Fe_{10}Si_{10}$. Mater. Char. *158*, 109947. https://doi.org/10.1016/j.matchar.2019.109947.

16. Jiang, J.C., Wang, N., Fung, K.K., and Kuo, K.H. (1991). Direct observation of domains and discommensurations in Mn-Si-Al octagonal quasicrystal by transmission electron microscopy. Phys. Rev. Lett. *67*, 1302–1305. https://doi.org/10.1103/PhysRevLett.67.1302.

17. Jiang, J.C., Fung, K.K., and Kuo, K.H. (1992). Discommensurate microstructures in phason-strained octagonal quasicrystal phases of Mo-Cr-Ni. Phys. Rev. Lett. *68*, 616–619. https://doi.org/10.1103/PhysRevLett.68.616.

18. Klein, H., Feuerbacher, M., Schall, P., and Urban, K. (1999). Novel type of dislocation in an Al-Pd-Mn quasicrystal approximant. Phys. Rev. Lett. *82*, 3468–3471. https://doi.org/10.1103/PhysRevLett.82.3468.

19. Piao, S., and Lidin, S. (2007). Occupation waves the way you have never seen them: the orthorhombic quasicrystal approximants $RE_{13}Zn_{58+\delta}$ (RE = Ho, Er, Tm, and Lu). Inorg. Chem. *46*, 6452–6463. https://doi.org/10.1021/ic700476w.

20. Duguet, T., Ünal, B., Ledieu, J., Dubois, J.M., Fournée, V., and Thiel, P.A. (2011). Nanodomains due to phason defects at a quasicrystal surface. Phys. Rev. Lett. *106*, 076101. https://doi.org/10.1103/PhysRevLett.106.076101.

21. He, Z., Li, H., Ma, H., and Ma, X. (2019). Hexagonal structural block consisting of 2 nm decagonal clusters in $Al_{60}Cr_{20}Fe_{10}Si_{10}$ alloy. J. Alloys Compd. *788*, 685–689. https://doi.org/10.1016/j.jallcom.2019.02.278.

22. Yang, L., Heggen, M., Feuerbacher, M., Han, X., and Dunin-Borkowski, R.E. (2022). Metadislocation configurations and novel phason defects in the complex metallic alloy T-Al-Mn-Pd. Acta Mater. *241*, 118388. https://doi.org/10.1016/j.actamat.2022.118388.

23. He, Z., Shen, Y., Ma, H., Sun, J., Ma, X., Li, H., and Steurer, W. (2020). Quasicrystal-related mosaics with periodic lattices interlaid with aperiodic tiles. Acta Crystallogr. A *76*, 137–144. https://doi.org/10.1107/S2053273320000066.

24. Honal, M., Haibach, T., and Steurer, W. (1998). Geometrical model of the phase transformation of decagonal Al-Co-Ni to its periodic approximant. Acta Crystallogr. A *54*, 374–387. https://doi.org/10.1107/S0108767397018837.

25. Inoue, A., Kimura, H.M., and Masumoto, T. (1987). Formation of Al-Cr-Si quasicrystal with high silicon concentration by rapid quenching and its thermal and electrical properties. J. Mater. Sci. *22*, 1864–1868. https://doi.org/10.1007/bf01132418.

26. Zhang, H., Wang, D.H., and Kuo, K.H. (1989). Icosahedral and decagonal quasicrystals, crystalline phases, and multiple twins in rapidly solidified $Al_{13}Cr_4Si_4$. J. Mater. Sci. *24*, 2981–2986. https://doi.org/10.1007/BF02385657.

27. Chen, H.L., Weitzer, F., Schuster, J.C., Du, Y., and Xu, H. (2007). The isothermal section of the Al-Cr-Si system at 800℃ and the crystal structure of τ_2 (Cr_3Al_9Si). J. Alloys Compd. *436*, 313–318. https://doi.org/10.1016/j.jallcom.2006.07.038.

28. Lu, P.J., and Steinhardt, P.J. (2007). Decagonal and quasi-crystalline tilings in medieval Islamic architecture. Science *315*, 1106–1110. https://doi.org/10.1126/science.1135491.

29. Cooper, M.J. (1960). The structure of the intermetallic phase θ(Cr-Al). Acta Crystallogr. *13*, 257–263. https://doi.org/10.1107/S0365110X60000571.

30. Chen, H., Wang, Q., Wang, Y., Qiang, J., and Dong, C. (2010). Composition rule for Al-transition metal binary quasicrystals. Philos. Mag. A *90*, 3935–3946. https://doi.org/10.1080/14786435.2010.502144.

31. Gummelt, P. (1996). Penrose tilings as coverings of congruent decagons. Geom. Dedicata *62*, 1–17. https://doi.org/10.1007/BF00239998.

32. Gummelt, P., and Bandt, C. (2000). A cluster approach to random Penrose tilings. Mater. Sci. Eng. *294–296*, 250–253. https://doi.org/10.1016/S0921-5093(00)01197-7.

33. Edagawa, K., Suzuki, K., and Takeuchi, S. (2000). High resolution transmission electron microscopy observation of thermally fluctuating phasons in decagonal Al-Cu-Co. Phys. Rev. Lett. *85*, 1674–1677. https://doi.org/10.1103/PhysRevLett.85.1674.

34. He, Z., Maurice, J.L., Ma, H., Wang, Y., Li, H., Zhang, T., Ma, X., and Steurer, W. (2021). Experimental observation of carousel-like phason flips in the decagonal quasicrystal $Al_{60}Cr_{20}Fe_{10}Si_{10}$. Acta Crystallogr. A *77*, 355–361. https://doi.org/10.1107/S2053273321007518.